Nanoscale

Accepted Manuscript

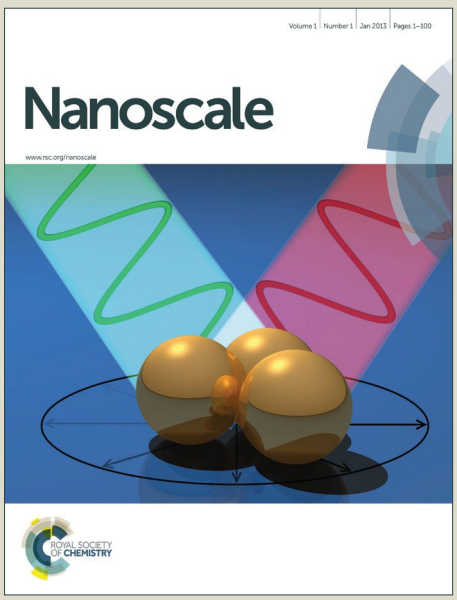

ROYAL SOCIETY OF CHEMISTRY

www.rsc.org/nanoscale

Cite this: DOI: 10.1039/c0xx00000x

www.rsc.org/xxxxxx

PAPER

Nanoparticles Cluster Gas Sensor: Pt Activated SnO_2 Nanoparticle for NH_3 Detection with Ultrahigh Sensitivity

Xu Liu,[a] Nan Chen,[a] Bingqian Han,[a] Xuechun Xiao,[a,b] Gang Chen,[a,b] Igor Djerdj[c] and Yude Wang*[a,b]

Received (in XXX, XXX) Xth XXXXXXXXX 20XX, Accepted Xth XXXXXXXXX 20XX

DOI: 10.1039/b000000x

Pt activated SnO_2 nanoparticle clusters were synthesized by a simple solvothermal method. The structure, morphology, chemical state and specific surface area were analyzed by X-ray powder diffraction (XRD), transmission electron microscopy (TEM), X-ray photoelectron spectrum (XPS) and N_2-sorption isotherm, respectively. The SnO_2 nanoparticle cluster matrix consists of tens thousands of SnO_2 nanoparticles with an ultra-small grain size estimated to be 3.0 nm. And there are abundant random-packed wormhole-like pores caused by the inter-connection of SnO_2 nanoparticles in whole of the cluster. The platinum element presents two forms including metal (Pt) and tetravalent metal oxide (PtO_2) in the Pt activated SnO_2 nanoparticle clusters. The as-synthesized pure and Pt activated SnO_2 nanoparticle clusters were used to fabricate gas sensor devices. It is found that the gas response toward 500 ppm ammonia is improved from 6.48 to 203.44 through the activation by Pt. And the results indicate that the sensor based on Pt activated SnO_2 not only has ultrahigh sensitivity but also possesses good response-recovery property, linear dependence, repeatability, selectivity and long-term stability, demonstrating the potential of using Pt activated SnO_2 nanoparticle clusters for ammonia gas sensing. At the same time, the formation mechanisms of the unique nanoparticle clusters and highly enhanced sensitivity are also brought out.

1. Introduction

Ammonia (NH_3), one of the most important industrial raw materials in the world, is widely used in the production of fertilizer, chemicals, textiles, and paper products.[1] Its global production exceeds 100 million tons per year.[2] Such a colorless gas with pungent odor is not only harmful to human's health but also has negative impact on the surrounding environment and ecosystem.[1,3] For example, NH_3 has strong irritation to eye, nose, throat as well as skin, which can lead to vomit, headache, pneumonedema and even death. Several safety standards toward NH_3 have been set up. For instance, the immediately dangerous to life or health concentration (IDLH) is stipulated to be 300 ppm by American National Institute for Occupational Safety and Health. The specified threshold limit value in the work place is 50 ppm stipulated by Occupational Safety and Health Administration (OSHA). The superfluous ammonia also leads to pollution of water and soil, which results in further harm toward aquatic organisms and terrestrial plants. Owning to the low-density and effumability natures of ammonia, the affected area would be quite large once the leakage of ammonia happened. Therefore, effective method to monitor NH_3 has been demanded for precise process control and atmospheric environmental measurements. To fabricate NH_3 gas sensor is thought to be a desirable means for monitoring it in corresponding environments, such as laboratory, factory and public place.

Since the gas sensing effect of Ge was uncovered by Brattain et al. around 1953, the field of gas sensing material, especially for metal oxide semiconductor (MOS), has gained great focusing on global scale and rapid development.[2,4] A series of promising sensing materials or matrix, such as SnO_2, ZnO, Fe_2O_3, WO_3, In_2O_3, TiO_2 and so on, have been reported for using of gas sensor owning to the abundant microstructural defects which are beneficial to forming absorbed oxygen ions.[5] Among them, SnO_2, an n-type semiconductor oxide, is the most promising and frequently used sensing material due to its low cost, high sensitivity and quick response.[6] However, the sensitivity of pure SnO_2 toward NH_3 is too poor to meet the standard of the demands. For example, Wei et al. reported that the response of mesoporous SnO_2 toward 500 ppm NH_3 is lower than 5.[7] Sheng et al. reported that the response of nanowire-like networks SnO_2 toward 100 ppm NH_3 is lower than 2.[8] It is also reported that the response of hexagonal SnO_2 nanoparticles toward 100 ppm NH_3 can not reach 3.[9] It has demonstrated that the sensitivity can be effectively improved by composing of noble metal such as Rh, Au, Pt, Pd and so on.[10] And the researches on noble metal and SnO_2 system used for detection of ammonia have been carried out. It is found that Pt is the most suitable one to enhance the sensitivity of SnO_2 toward NH_3, and the response toward 450 ppm NH_3 is improved from 1.33 to 25.7.[6] Wang et al. reported that the response toward 200 ppm NH_3 is improved from 2 to 25 with addition of Pt into SnO_2 powder.[11] However, the NH_3 response around 25 towards a high concentration of 200 or 450 ppm is still un-ideal, and more efforts in its design and engineering for high sensitivity level toward ammonia are needed.

As we know, the enhancement of gas response caused by addition of platinum can be attributed to two main reasons: catalytic promotion obtained by platinum and the extension of the space-charge layer, which result from metal-semiconductor contact of Pt-SnO_2 and p-n junction of PtO_x-SnO_2 (x=1,2).[12] And it is also known to us that the sensing reactions mainly occur on the interface between SnO_2 and target gases.[13] These mean only the Pt (or PtO_x) decorating on the surface of SnO_2 can show its function. In another words, providing a high surface area for Pt (or PtO_x) to attach might lead to a highly improved sensitivity. From the perspective of theory, the nanoparticle ought to have the highest surface area in the same amount of mass, and it will be higher with smaller grain size. Nevertheless, high agglomerations are always observed in nanoparticles owing to the high surface energy which is the nature of nanomaterials. It not only leads to a low specific surface area but also causes a poor structural stability, which results in the un-ideal sensing properties including sensitivity, repeatability and long-term stability. It has been proven that assembling nanosized structure onto lager sized structure can be effective to minimize the agglomeration because the assembled larger sized structures possess a superior structural stability.[14] Hence, assembling the SnO_2 nanoparticles with controllable small grain size to larger sized structure used as matrix for Pt-SnO_2 system could be a good choice to obtain a high sensitive sensor toward ammonia. However, most reported literatures about such the assembled structure focus on the novel morphology of final assembled structure rather than the turning of primary units,[15] leading to an un-ideal gas sensing properties.

Herein, we describe a simple solvothermal route to Pt activated SnO_2 nanoparticle clusters for NH_3 sensing purposes. The SnO_2 cluster matrix consists of tens thousands of SnO_2 nanoparticles with an ultra-small grain size about 3.0 nm. The inter-connection of the SnO_2 nanoparticles leads to random-packed wormhole-like porous in the whole of SnO_2 nanoparticle cluster, which results in a high specific surface area (181.58 m^2g^{-1}). The obtained Pt activated SnO_2 nanoparticle clusters were used to fabricate gas sensor which shows good sensing properties toward NH_3, especially for the ultra-high sensitivity. To be more specific, the gas response toward 500 ppm NH_3 reaches as high as 203.44. The structure, morphology and chemical state are also investigated to give a further understanding of related mechanisms of nanoparticle cluster formation and gas sensing.

2. Experimental section

2.1 Preparation of Pt activated SnO_2 nanoparticle clusters

All the chemical reagents used in the experiments were obtained from commercial sources as guaranteed-grade reagents and used without further purification.

Pt activated SnO_2 nanoparticle clusters were synthesized by a simple solvothermal method. In a typical synthetic experiment, 0.8167 g stannic chloride pentahydrate ($SnCl_4{\cdot}5H_2O$), 0.62 mL ethylenediamine ($C_2H_8N_2$) and 0.58 mL chloroplatinic acid (H_2PtCl_6) aqueous solution (0.1214 M) were dissolved into 20, 10 and 5 mL methanol to form transparent solutions, respectively. Later, chloroplatinic acid solution was poured into stannic chloride solution. After magnetically stirring for 15 min, the solution of ethylenediamine was added, and a light yellow suspension is obtained. 30 mL of the suspension was transferred into a Teflon-lined stainless steel autoclave with a capacity of 35 mL and reacted under solvothermal condition at 150 ºC for 24 h. The autoclave was cooled down to room temperature in standard atmosphere. The resulting products were centrifuged, and the precipitates were thoroughly washed with ethanol and dried at 60 ºC overnight. Pt activated SnO_2 nanoparticles with a theoretical Pt load of 3 at.% ([Pt]/[Sn]) were synthesized because the ratio was found to be the most promising for the gas sensing performances in our incipient experiments. The pure SnO_2 sample was also synthesized by the same process without the use of chloroplatinic acid.

2.2 Characterization of as-prepared samples

X-Ray diffraction (XRD, Rigaku D/MAX-3B powder diffractometer) with a copper target and K_α radiation (λ=1.54056 Å) was used for the phase identification, where the diffracted X-ray intensities were recorded as a function of 2θ. The sample was scanned from 10° to 90° (2θ) in steps of 0.02°. The transmission electron micrographs (TEM) were obtained with a Zeiss EM 912 Ω instrument at an acceleration voltage of 120 kV, while high-resolution transmission electron microscopy (HRTEM) characterization was done using a Philips CM200-FEG microscope (200 kV, C_s=1.35 mm). The samples for TEM were prepared by dispersing the final dry powders in ethanol; this dispersion was then dropped on carbon-copper grids. Nitrogen adsorption isotherm was measured at 77.3 K with a Micromeritics ASAP 2010 automated sorption analyzer. Prior to the measurement, the sample was degassed at 300 °C for 3 h under vacuum. X-ray photoelectron spectroscopy (XPS) was carried out at room temperature in ESCALAB 250 system. During XPS analysis, an Al Kα X-ray beam was adopted as the excitation source and the vacuum pressure of the instrument chamber was 1×10^{-7} Pa as read on the panel. Measured spectra were decomposed into Gaussian components by a least-square fitting method. Bonding energy was calibrated with reference to C1s peak (285.0 eV).

2.3. Fabrication and measurement of gas sensor

The sensor of indirect heating was fabricated according to the literature.[16] At the very beginning, the as-synthesized products were mixed with an appropriate deionized water to form a paste. Afterwards, the paste was coated by a paint pen onto the outside surface of an alumina tube (4 mm in length, 1.2 mm in external diameter, and 0.8 mm in internal diameter) with a pair of Au electrodes at each end connected by platinum wires. The thickness of the gas sensing materials is measured to be 0.6-0.8 mm to uniformly cover the whole Au electrodes to guarantee a good contact. Next, the sensors were calcined in air at 400 ºC for 2 h and then a Ni-Cr heating wire was inserted in the tube to control the operating temperature via a heating voltage (V_h), as shown in Fig. S1. In order to improve the stability and repeatability, the fabricated sensors were aged at 320 ºC for 48 h in air. Finally, the sensors were well connected to bakelite base through platinum wires to perform electrical measurements using a WS-30 A system (Weisheng Instruments Co. Zhengzhou, China, as seen in Fig. S1). During the testing process, the desired amounts of target substance were injected into the chamber by a microsyringe after the resistances of all the sensors were stable.

The analyte solution was evaporated by a quick evaporator and mixed with air immediately by two installed fans in the chamber (18 L in volume). The gas response β was defined as the ratio of the electrical resistance in air (R_0) to that in gas (R_g). In addition, the response time was defined as the time required for the gas response reaching 90% of the final equilibrium value after a test gas was injected, and the recovery time was the time needed for gas response decreasing its 90% after the gas sensor was exposed in air again.

3. RESULTS AND DISCUSSION

X-ray diffraction analysis of as-synthesized samples was carried out for phase identification, and the results are shown in Fig. 1. The curve b exhibits the XRD pattern of SnO_2 nanoparticle clusters. Obviously that all the reflections of the pattern can be identified as the reflections of cassiterite SnO_2 (JCPDS Card No. 41-1445), space group $P4_2/mnm$ (136). Owing to the broadening of diffraction peaks, the overlapping of neighboring peaks can be observed in whole of the pattern. Comparing pattern b with c, one can find that the addition of chloroplatinic acid leads to the appearance of three new peaks which center at 39.78°, 43.44° and 46.28° respectively. The peaks centered at 39.78° and 46.28° correspond to (111) and (200) reflections of Pt (JCPDS Card No.65-2868), respectively. And the peak at 43.44° can be identified as the reflection of (004) lattice plane belonging to PtO_2 (JCPDS Card No. 73-2360). At the same time, it can be found that the major peaks of PtO_2, such as (002) and (101), were not observed in the pattern c. This phenomenon might results from the (004) preferred orientation of PtO_2. These mean that the platinum element presents two forms including metal (Pt) and tetravalent metal oxide (PtO_2) in the Pt activated SnO_2 nanoparticle clusters.

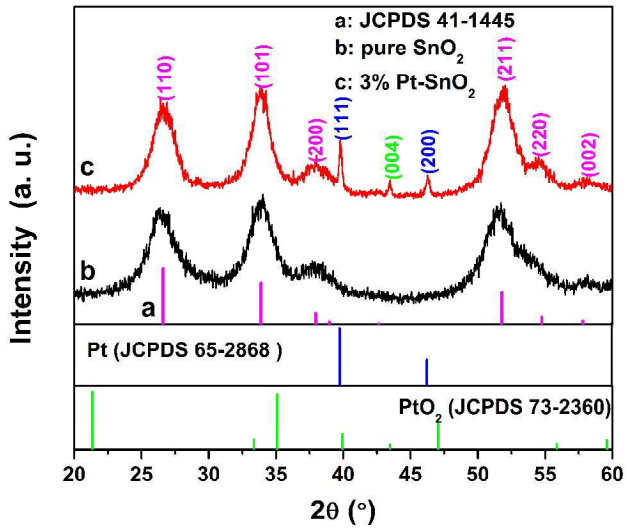

Fig. 1 XRD patterns of as-synthesized pure and Pt activated SnO_2 nanoparticle clusters.

To have a better understanding of the structural features of the as-synthesized SnO_2 nanoparticle cluster matrix, the initial assignment is further confirmed by the refinement of the diffraction patterns with the Rietveld method.[17] The experimental pattern, together with the calculated pattern obtained from Rietveld refinement and difference profiles are shown in Fig. 2. Its average crystallite size calculated to be 3.0 nm. And the other structural parameters obtained from Rietveld profile refinement such as unit cell parameters, fractional atomic coordinates, and microstrin are listed in Table S1. The significant line broadening due to the small crystallite sizes and microstrain brought in by the heterosubstitution influenced the final agreement between experimental and calculated patterns. However, the calculated and experimental XRD patterns are in satisfactory agreement from the difference curve.

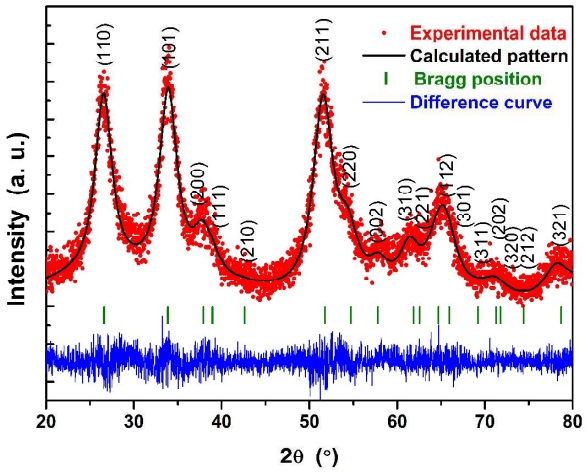

Fig. 2 Typical Rietveld output plot of as-synthesized SnO_2 nanoparticle clusters. The experimental data, calculated pattern and the difference curve are shown in red, black and blue, respectively. The short vertical bars in green represent the positions of the Bragg reflections.

The morphology of as-prepared Pt activated SnO_2 nanoparticle clusters were further examined with transmission electron microscopy (TEM) as shown in Fig. 3. In Fig. 3 (a), a large cluster can be found, and there randomly distributes countless wormhole-like pores in the cluster. To have a further understanding of its microstructure, a magnified TEM imagine of the edge part marked by black dash line in Fig. 3(a) is displayed in Fig. 3(b). From the magnified TEM imagine, one can find that the huge cluster consists of tens thousands of ultra-small SnO_2 nanoparticles, and the formation of wormhole-like pores can be attributed to the inter-connection of the nanoparticles. Moreover, such the morphological feature can be observed in the whole of cluster in Fig. S2 (a) which presents an unbroken nanoparticle cluster with a size around 600 nm and irregular shape. The TEM imagine of an as-synthesized pure SnO_2 nanoparticle cluster presents a similar feature to Pt activated sample (Fig. S2 (b)). The high-resolution TEM (HRTEM) image of Pt activated SnO_2 nanoparticle cluster is shown in Fig. 3(c), the clear well-developed lattice fringes imply a high crystallinity and random orientation of the SnO_2 nanoparticles. At the same time, it can be found that the size of SnO_2 nanaoparticles mostly falls in 2 to 4 nm. And in the selected-area electron-diffraction (SAED) pattern (inset in Fig. 3(c)), four broadening characteristic diffraction rings corresponding to the reflections (110), (101), (211) and (301) of cassiterite SnO_2 also demonstrates the ultra-small grain size of the SnO_2 nanoparticles. Owing to the inter-connection

feature of the SnO_2 nanoparticles making up the matrix, the particles of platinum and platinum dioxide are hard to be observed. But the strong diffraction peaks at 39.78°, 43.44° and 46.28° in Fig. 2(c) have been strong enough to prove the existence of platinum-related phase in Pt activated SnO_2 nanoparticle clusters. A HRTEM imagine of an isolated SnO_2 nanoparticle is also displayed in Fig. 3(d). The interplanar spacing is estimated to be 0.335 nm, which is close to (110) lattice plane of SnO_2. The size of such a well-defined particle can be easily measured to be 3.1 nm, which has a good agreement with the result of XRD.

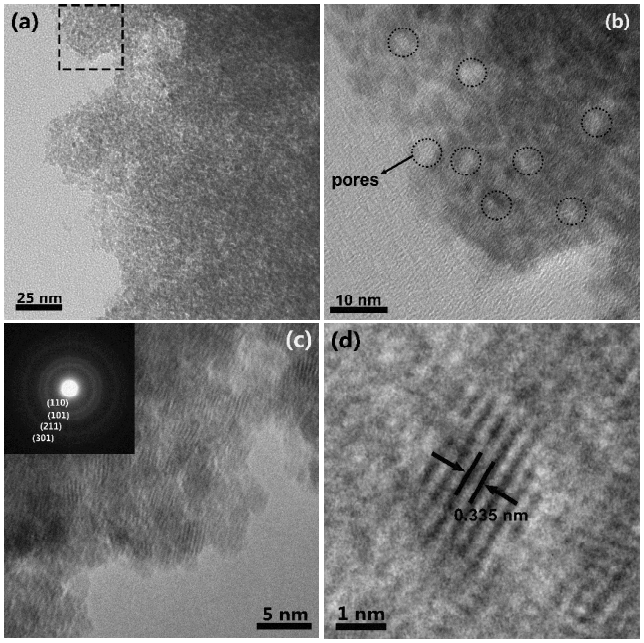

Fig. 3 (a) TEM image and (b) magnified TEM image of of Pt activated SnO_2 nanoparticle clusters, HRTEM image of (c) Pt activated SnO_2 nanoparticle clusters and (d) an isolated SnO_2 nanopaticle. Inset is the selected area electron diffraction of Pt activated SnO_2 nanoparticle clusters.

N_2-adsorption isotherm was also carried out toward as-synthesized Pt activated SnO_2 nanoparticle clusters, and the specific surface area estimated from BET method is 181.58 m^2g^{-1}. Such a high specific surface area is attributed to the synergy of ultra-small grain and assembled microstructure, which is highly depending on the synthetic method. And the formation mechanism of the SnO_2 nanoparticle cluster matrix can be described as Fig. 4. At the first, stannic chloride and ethylenediamine produce Sn^{4+} and OH^- respectively in the solvents through ionization. The ionized Sn^{4+} and OH^- react to form $Sn(OH)_4$. The later process that the formation of SnO_2 crystal nuclei from $Sn(OH)_4$ is quite complicated, however, it mainly depends on the dehydration of $Sn(OH)_4$.[18] At the same time, the surface of SnO_2 crystal nuclei is capped by hydroxide ions which can form hydrogen bonds with methanol, and the methyl showing positive electricity points to the solvent. The methyl is stable with $Sn(OH)_4$ dissociating in the solvent, which means methanol acts as an inhibitor to limit the growth of SnO_2.[19] On the other hand, unionized ethylenediamine also can form hydrogen bond with the hydroxide ions bonded at the surface of SnO_2 crystal nuclei. Owing to the symmetrical structure of ethylenediamine, the two nitrogen-atoms with high negative electricity at the both ends of ethylenediamine can form hydrogen bonds, which gives it a possibility to link two SnO_2 crystal nuclei. With a further connection and limited growth, the unique SnO_2 nanoparticle cluster was formed. Because the formation of hydrogen bond between ethylenediamine and SnO_2 nanoparticles is random, the connection of SnO_2 nanoparticles is random too, which leads to the randomly distribution and irregular shape of the pores. At the same time, the acting force of the formed hydrogen bond only exists between the nanoparticles, so the shape of the cluster is irregular. The catalyst loading of Pt and PtO_2 could be explained in a similar process which can be represented by the follows:[20]

$$Pt^{4+}+Sn^{4+}+8OH^- = SnO_2/PtO_2+4H_2O \quad (1)$$

$$SnO_2/PtO_2 \xrightarrow[\text{solvothermal}]{\text{methanol}} Pt/SnO_2 \quad (2)$$

Pt^{4+} and Sn^{4+} react with OH^- to form corresponding hydroxides which further transforms to SnO_2/PtO_2. Then formed PtO_2 will be reduced by methanol in the solvothermal surrounding gradually.

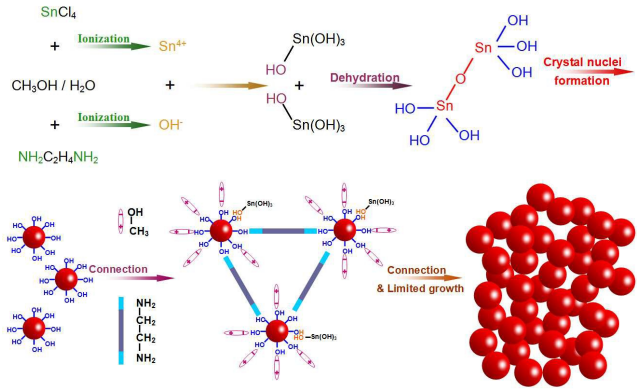

Fig. 4 Schematic illustration of the formation process of the SnO_2 nanaoparticle cluster matrix.

According to the analysis of the possible formation mechanism of the SnO_2 nanoparticle cluster matrix, one can find that the formed hydrogen bonds act an essential role. And the formation of hydrogen bond is highly relied on the hydrogen ionize bonded at the surface of SnO_2 nanoparticles. As we know, the existence of formed hydrogen can be sensitively detected by X-ray photoelectron spectroscopy (XPS). Hence, XPS was carried out to study the chemical composition of as-synthesized Pt-activated SnO_2 nanoparticle clusters. Apart from the peak of C1s at 285 eV, only the peaks related to Sn, O and Pt can be observed in Fig. S3(a), indicating a good purity of as-synthesized samples. Sn3d spectra (Fig. S3(b)) reveal two peaks of $Sn3d_{3/2}$ and $Sn_{3d5/2}$ with a good symmetry and the splitting of 3d doublet is 8.39 eV, demonstrating that Sn in the nanoparticle clusters is in a single form of Sn^{4+}.[16] Fig. 5(a) displays the high-resolution Pt4f XPS spectra. $Pt4f_{5/2}$ and $Pt4f_{7/2}$ peaks are observed at 74.4 and 71.07 eV respectively, illustrating the nature of metal platinum.[12] A low signal-noise ratio is also observed in the figure, which is thought should be responsible for the disappearing signal of Pt^{4+}. High-resolution XPS spectra of O1s were shown in Fig. 5(b), one can find that the O1s consists of three components in different chemical states: O_{latt} (530.73 eV), O_x^- (531.71 eV) and O_{OH}

(533.02 eV). O_{latt} is attributed to oxygen ions in the crystal lattice which are thought to be pretty stable and have no contribution to the gas response, meanwhile, O_x^- is the absorbed oxygen ions which take a very important role in the gas sensing property and will be further discussed in the sensing mechanism section in the oxygen deficient regions such as oxygen vacancy (V_O), oxygen interstitial (O_i) and oxygen antisite (O_{Sn}).[21] And the peak centered at 533.02 eV has been suggested to be assigned to the hydroxyl ions on the surface.[22] Through calculating the ratio of peak area, the concentrations of O_{latt}, O_x^- and O_{OH} in reference of O1s are estimated to be 19.8%, 30.8% and 49.4%, respectively. The high concentration of O_{OH} indicates the existence of a mass of hydroxyl ions on the surface of the SnO_2 nanoparticles, which supports the formation mechanism brought up above to some agree.

In the XRD data, Pt and PtO_2 characteristic peaks were clearly observed. However, Pt and PtO_2 were not observed in HRTEM images and SAED pattern. In addition, Pt related peaks were very weak in XPS analysis, and even Pt^{4+} peaks were not observed. These phenomena can be explained from two aspects: The structural as well as morphological natures of the Pt-SnO_2 nanoparticle clusters, and the natures of different detecting methods. The SnO_2 nanoparticles have linked to huge clusters (Fig. 3) which means there is a possibility that Pt and PtO_2 were coated by the SnO_2 nanoparticles, meanwhile the ratio of [Pt]/[Sn] is only 3 at.% which is a very low level. These two reasons cause the Pt and PtO_2 were not observed in HRTEM images. Apart from these, the detection area of SAED is limited which means a strong randomness is hard to be avoided, and further leading to Pt and PtO_2 were not observed in SAED pattern. On the other hands, we know that the detection depth of XRD and XPS has much difference. As to Pt-SnO_2 materials, the detection depth of XRD with a Cu target is around 10 μm, while the detection depth of XPS with an Al target only reaches 5 nm. 10μm is much bigger than the scale of the clusters, but 5 nm only reaches the surface of the clusters. That is to say XRD with a deeper detection depth shows the structural features of the samples while XPS with a shallow detection depth only displays the surface feature. As we have announced that there is a possibility that the Pt and PtO_2 are capped by the SnO_2 nanoparticles, and the ratio [Pt]/[Sn] is very small which further decrease the possibility that observe Pt and PtO_2 on the surface of the clusters. Hence, the characteristic peaks of Pt and PtO_2 can be obviously observed in XPD pattern, but the signal of Pt^{4+} (PtO_2) is not found by XPS.

To evaluate the potential applicability in gas sensor for ammonia, some fundamental gas sensing properties of as-prepared samples were investigated. It is known to us that the operating temperature has a great influence on sensing properties especially for the sensitivity. There usually exist a temperature region in which sensor shows the highest gas response under the same other conditions. Fig. 6 depicts the relation between the response and the operating temperature for both pure and Pt activated SnO_2 nanoparticle clusters toward 500 ppm ammonia. Obviously that the Pt activated sample has much higher sensitivity. The gas response toward 500 ppm is greatly promoted from 6.48 to 203.44 through the activation by Pt. At the same time, the most sensitive operating temperature is shift from 140 °C to 115 °C.

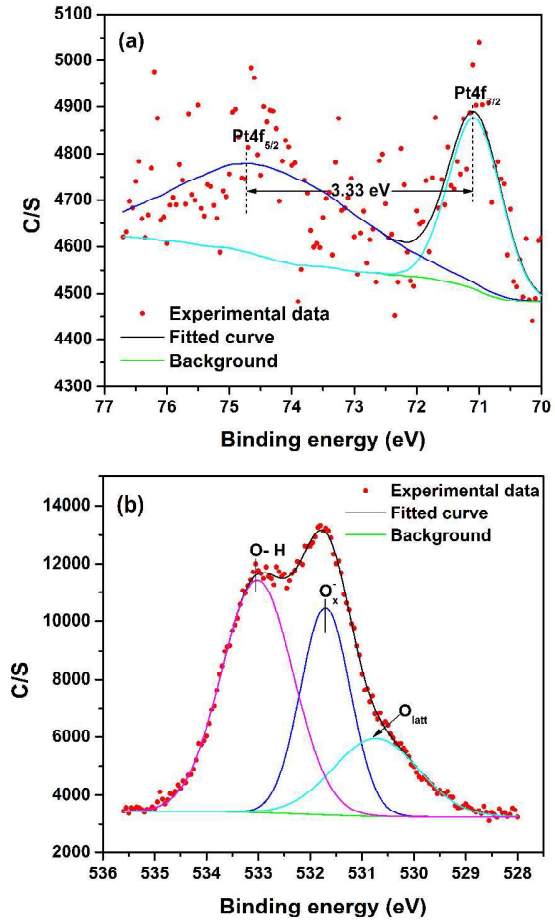

Fig. 5 High-resolution XPS spectra of (a) Pt4f and (b) O1s for Pt activated SnO_2 nanoparticle clusters.

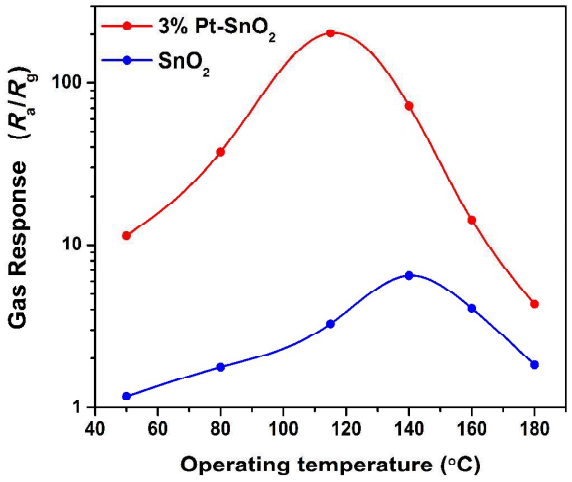

Fig. 6 Gas response of the sensors based on pure and Pt activated SnO_2 nanoparticle clusters toward 500 ppm ammonia at different operating temperature.

These phenomena including higher sensitivity and lower optimal operating temperature are thought to be the typical characteristics of noble metal activation in gas sensing property, which in turn directly verifies the promoted effect of Pt functionalization.[2,10a,12a,21,23] And in the coming investigation on

the gas sensing properties of Pt activated SnO_2 nanoparticle clusters, 115 °C was chosen as operating temperature due to the highest sensitivity at that temperature.

Fig. 7(a) displays a dynamic response-recovery curve of Pt activated SnO_2 nanoparticle clusters toward different ammonia concentration from 50 to 1000 ppm, and a good response-recovery property can be observed. The gas response keeps almost constant with only small fluctuations when it reaches its dynamic balance in both air and ammonia. And the gas response can also rapidly increase and decrease in response and recovery situations, respectively. According to the definition of response/recovery time, the response and recovery time are calculated to be 75 s and 67 s (from Fig. S4), respectively. On the other hand, as-fabricated sensor based on Pt activated SnO_2 nanoparticle clusters surely possess an ultra-high sensitivity. More specifically, the gas responses toward 50, 100, 300, 500, 700, and 1000 ppm ammonia are 29.19, 69.17, 150.44, 203.44, 249.29, and 314.43, respectively. Apart from these, the gas response toward 10 ppm ammonia is also tested and the value is calculated to be 4.3. Because the response toward 10 ppm ammonia is much smaller than that of those high concentrations, the response is hard to show in Fig. 7(a) together with others. Hence the dynamic response-recovery toward 10 ppm is shown in Fig. S5 alone. As we have announced in the introduction, the two limits of ammonia are 50 and 300 ppm. Hence the fabricated gas sensor based on Pt activated SnO_2 nanoparticle clusters is quite sensitive to ammonia, and its gas response is well satisfied with the detection needs. The linear dependence of gas response on the gas concentration is also investigated as shown in Fig. 7(b), the experimental data in range from 100 to 1000 ppm were fitted as:

$$\lg \beta = 0.5386 + 0.6550 \lg C \qquad (3)$$

where β is the gas response and C is the concentration of ammonia. The correlative coefficient R^2 is 0.9984 indicating a good linear dependence.

Repeatability is one important parameter which can be used to evaluate the reliability of the fabricated sensor. So, the repeatability of as-fabricated sensor was investigated by testing 300 ppm ammonia for five times under same conditions, and the dynamic response-recovery curve was shown in Fig. 7(c). The gas response in every test reaches around 150 with small fluctuations which are estimated to be 4.1%, and the response/recovery time does not have distinct difference. Both of them indicate that the as-fabricated ammonia sensor based on Pt activated SnO_2 nanoparticle clusters has a good repeatability. At the same time, the response to some common VOCs such as acetone, ethanol, formaldehyde and isopropanol with a concentration of 100 ppm was also measured at 115 °C. The dynamic resistance-time curves are shown in Fig. S6, and the values are summarized in Fig. 7(d). It is obvious that the sensitivity toward ammonia is the highest than that of the other gases for as-fabricated sensor. The gas response toward ammonia is roughly 15.2, 7.4, 5.8, 12.3 times higher than that toward acetone, ethanol, formaldehyde and isopropanol, respectively. It means the gas sensor based Pt activated SnO_2 nanoparticle clusters exhibits a good selectivity toward ammonia.

Table 1 shows a brief summary of the sensing performances of various SnO_2 based gas sensor toward ammonia. As it has been introduced, the sensitivity of pure SnO_2 toward ammonia is poor. And the sensitivity of pure SnO_2 nanoparticle clusters does not have much difference with that of the regular SnO_2 materials such as hexagonal SnO_2 nanoparticles, SnO_2 nanowire-like networks, mesoporous SnO_2 and SnO_2 nanofibers.[7,8,9,24] By doping and composing SnO_2 with some enhancer can significant promote its sensitivity, especially for the composing of noble metal such as Pd and Pt. And the as-synthesized Pt activated SnO_2 nanoparticle clusters in this work shows the highest gas response. For the Pt activated SnO_2 thin film reported in 2nd and 27st reference, the Pt enhancer only appears on the surface of the SnO_2 matrix film which surface area is limited. At the same time, the Pt-doped SnO_2 powder (13th reference) is prepared by chemical precipitation method following sintering which leads to a hard agglomeration and unlimited growth. Hence their sensitivity is still un-ideal. But for the as-fabricated Pt activated SnO_2 nanoparticle clusters, inter-connection of the SnO_2 nanoparticles with controllable ultra-small grain size leads to the formation of abundant pores and assembled larger sized structure, which further results in a high specific surface area for Pt to decorating and showing its function.

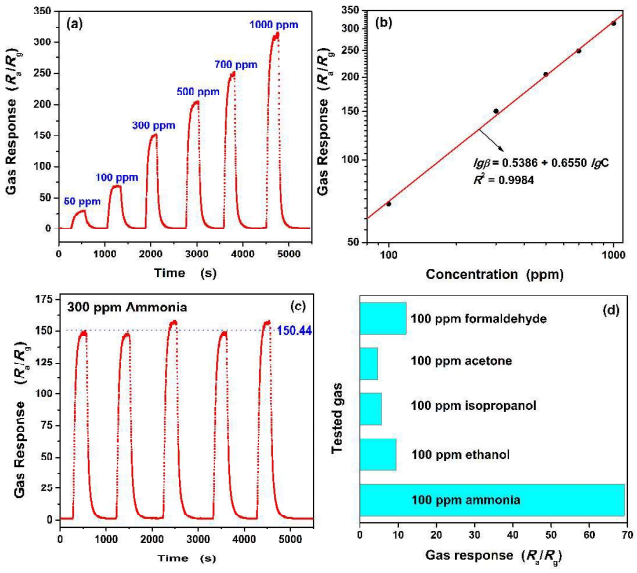

Fig. 7 The gas sensing properties of the sensor based on Pt activated SnO_2 nanoparticle clusters at an operating temperature of 115 °C. (a) Dynamic response-recovery curve toward different ammonia concentration from 50 to 1000 ppm, (b) variation of gas response to different ammonia concentration from 100 to 1000 ppm, (c)dynamic response-recovery cycles toward 300 ppm ammonia, and (d) gas response toward different gases with a concentration of 100 ppm.

In practical application, the long-term stability of gas sensor is also one important parameter to determine its reliability and service life. To verify the long-term stability of the as-fabricated sensor, the gas response evolution toward 500 ppm ammonia were tested and shown in Fig. 8. The relative deviation of the gas response in the first two weeks is estimated to be 9.3%. After 100 days, the relative deviation of the gas response in the coming two weeks is 10.01% which is very small too. Both of them indicate that the sensor surely posses a good long-term stability. And such a good stability also demonstrates a potential application in

ammonia detection.

Table 1 Comparison of the sensing performances of various SnO2 based gas sensor toward ammonia.

Materials	Concentration (ppm)	Operating temperature (°C)	Sensitivity	references
Hexagonal SnO_2 nanoparticles	46	100	<1.5	9
SnO_2 nanowire-like networks	100	300	<1.5	8
Mesoporous SnO_2	500	260	<5	7
SnO_2 nanofibers	100	280	≈14	24
Sb-doped SnO_2 nanoparticles	500	79	13.87	3
Polyprrole-coated SnO_2 hollow spheres	20	Room temperature	≈3.5	25
SnO_2/MWCNTs composite	600	Room temperature	≈50	26
Pt activated SnO_2 thin film	450	230	25.7	2
Pt-SnO_2 thin film	48	325	13	27
Pt-doped SnO_2 powder	200	160	25	11
Pd activated SnO_2 films	1000	60	68	28
Pt activated SnO_2 nanoparticle clusters	100 500 1000	115	69.17 203.44 314.43	This work

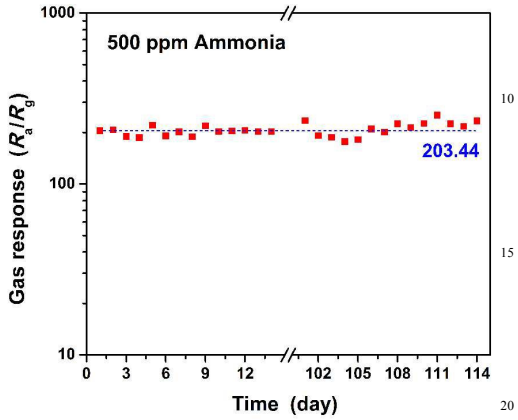

Fig. 8 The gas response of the sensor based on Pt activated SnO_2 nanoparticle clusters toward 500 ppm ammonia gas tested once a day at an operating temperature of 115 °C.

The detection mechanism of ammonia for the as-fabricated sensor is based on its changed conductance, which can be described by Wolkentein's model as shown in Fig. 9.[29] Through capturing free electrons from the sensing materials, oxygen species absorbed from the air onto the surface of SnO_2 nanoparticles can ionize to adsorbed oxygen ions (O_x^-), leading to the formation of a thick space-charge layer and a consequent high resistance of the sensor. This process can be described by the following equations:[13]

$$O_{2gas} \leftrightarrow O_{2ads} \quad (4)$$

$$O_{2ads} + e^- \leftrightarrow O_{2ads}^- \quad (5)$$

$$O_{2ads}^- + e^- \leftrightarrow 2O_{ads}^- \quad (6)$$

$$O_{ads}^- + e^- \leftrightarrow O_{ads}^{2-} \quad (7)$$

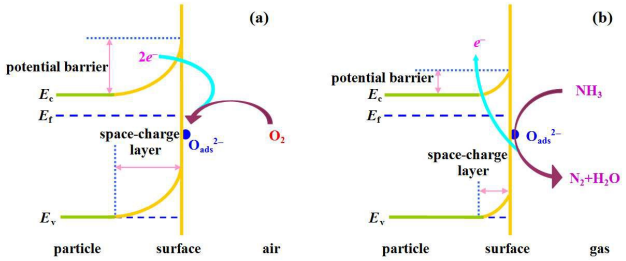

Fig. 9 Schematic diagram of the proposed reaction mechanism of Pt activated SnO_2 based sensor to ammonia in (a) air and (b) ammonia.

Once the sensor was exposed to ammonia, ammonia would react with adsorbed oxygen ions and the captured electrons would be released, leading to a thinner space-charge layer and lower potential barrier. This process results in decreasing of resistance and can be express as following equations:[3]

$$(NH_3)_{gas} \leftrightarrow (NH_3)_{ads} \quad (8)$$

$$2(NH_3)_{ads} + 3O^-_{ads} \rightarrow N_2 + 3H_2O + 3e^- \quad (9)$$

$$2(NH_3)_{ads} + 3O^{2-}_{ads} \rightarrow N_2 + 3H_2O + 6e^- \quad (10)$$

At the same time, it has been proven that there are abundant absorbed oxygen ions in the as-synthesized Pt activation SnO_2 nanoparticle cluster (in XPS section), which also indicates the reasonability of the sensing mechanism.

The significant enhancement of the sensitivity toward ammonia is attributed the synergistic effect of both matrix and enhancer. The enhancement caused by platinum can be explained by catalytic promotion and extension of space-charge layer. Apart from the catalytic promotion caused by the nature of noble metal and noble oxide, the enhanced mechanism of extension of space-charge layer can be explained by Wolkentein's model and described as Fig. 9. In the XRD section, it has concluded that the platinum element presents two forms including metal (Pt) and tetravalent metal oxide (PtO_2) in the Pt activated SnO_2 nanoparticle clusters. Owning to the high work function of metal platinum, the electrons belong to SnO_2 will transfer to metal platinum. And the p-type PtO_2 will form p-n junction with n-type SnO_2, which also leads to the transferring of electrons from SnO_2 to PtO_2. Both of them lead to extension of space-charge layer.[12] According to the sensing mechanism, extension of space-charge layer in the initial state will result in the promotion of sensitivity. On the other hand, the ultra-small size of SnO_2 and abundant pores of the matrix provide a high specific surface area for Pt and PtO_2 to decorating to show its function.

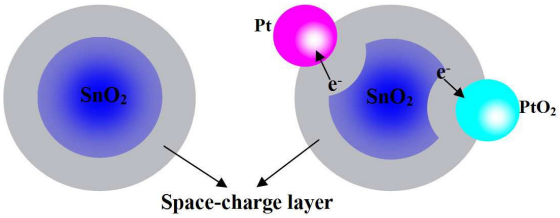

Fig. 10 Schematic diagram of the mechanism for the enhancement caused by metal-semiconductor and p-n junctions.

4. Conclusion

Pt activated SnO_2 nanoparticle clusters were successfully synthesized by a simple solvothermal method. Owing to the ultra-small grain size of SnO_2 nanoparticles which is the primary units of the clusters and the abundant pores caused by inter-connection of the nanaoparticles, the as-synthesized Pt activated SnO_2 nanoparticle clusters have a high specific surface area (181.58 m^2g^{-1}). Through forming hydrogen bonds with the hydroxyl ions covered on the surface of SnO_2 crystal nuclei, methanol and ethylenediamine act as growth inhibitor and bridging agent, which should be responsible for the ultra-small grain size and inter-connection of the SnO_2 nanoparticles, respectively. At the same time, it is found that the decorating of Pt-related phase can significant enhance the sensitivity of SnO_2 nanoparticle cluster matrix toward ammonia. Apart from the ultra-high sensitivity, the gas sensor based on as-synthesized Pt activated SnO_2 nanoparticle cluster also possess good response-recovery property, linear dependence, repeatability, selectivity and long-term stability, demonstrating the potential of using Pt activated SnO_2 nanoparticle clusters for ammonia gas sensing. The significant enhancement of the sensitivity toward ammonia is attributed to the synergistic effect of both matrix and enhancer. Pt-related phases as enhancer have catalytic promotion and lead to extension of space-charge layer. SnO_2 nanoparticle clusters (matrix) with a high specific surface area provide abundant sites for enhancer to decorate.

Acknowledgments

This work was supported by National Natural Science Foundation of China (Grant No.51262029), the Key Project of the Department of Education of Yunnan Province (ZD2013006), the Department of Science and Technology of Yunnan Province via the Key Project for the Science and Technology (Grant No.2011FA001), and National Training Program of Innovation and Entrepreneurship for Undergraduates (No. 201310673026).

Notes and references

[a] *School of Physical Science and Technology, Yunnan University, 650091 Kunming, People's Republic of China.*

[b] *Yunnan Province Key Lab of Micro-Nano Materials and Technology, Yunnan University, 650091 Kunming, People's Republic of China. E-mail: ydwang@ynu.edu.cn; Fax:+86-871-65153832;+86-871-65031124*

[c] *RuđerBošković Institute, Bijeni čka 54, 10000 Zagreb, Croatia. Fax: +38514680114; Tel: +38514680113; E-mail: igor.djerdj@irb.hr.*

† Electronic Supplementary Information (ESI) available: Table S1. structural data and refinement parameters for SnO_2 nanoparticle clusters calculated by Rietveld refinement; Fig. S1. The gas sensor and the testing principle diagram; Fig. S2. TEM images of investigated unbroken Pt activated and pure SnO_2 nanoparticle clusters; Fig. S3. XPS survey and high-resolution spectra of Sn3d for Pt activated SnO_2 nanoparticle clusters; Fig. S4. Magnified dynamic response-recovery curve toward 1000 ppm ammonia with labeled response/recovery time; Fig. S5. Dynamic Response/recovery versus time curve of as-fabricated sensor based on Pt-SnO_2 nanoparticles toward 10 ppm ammonia; Fig. S6. Dynamic Response/recovery versus time curve of as-fabricated sensor based on Pt-SnO_2 nanoparticles toward 100 ppm acetone, ethanol, formaldehyde and isopropanol. See DOI: 10.1039/b000000x/

1 X. Liang, Z. Chen, W. Hao, L. Gao, C. He, B. Wang and Y. Wu, *Carbon,* 2014, **80**, 268.

2 M. Shahabuddin, A. Sharma, J. Kumar, M. Tomar, A. U. Umar and V. Gupta, *Sensor. Actuat. B,* 2014, **194**, 410.

3 Y. Wang, Q. Mu, G. Wang and Z. Zhou, *Sensor. Actuat. B,* 2010, **145**, 847.

4 W. H. Brattain and J. Bardeen, *Bell Syst. Tech. J.,* 1953, **2086**, 1.

5 (a) Y. K. Chung, M. H. Kim, W. S. Um, H. S. Lee, J. K. Song, S. C. Choi, K. M. Yi, M. J. Lee and K. W. Chung, *Sensor. Actuat. B,* 1999, **60**, 49. (b) Q. Qi, P. P. Wang, J. Zhao, L. L. Feng, L. J. Zhou, R. F. Xuan, Y. P. Liu and G. D. Li, *Sensor. Actuat. B,* 2014, **194**, 440.

6 D. Hu, B. Han, S. J. Deng, Z. P. Feng, Y. Wang, J. Popoyic, M. Nuskol, Y. Wang and I. Djerdj, *J. Phys. Chem. C,* 2014, **118**, 9832.

7 W. Guo, X. C. Duan, Y. Shen, K. Qi, C. Wei and W. Zheng, *Phys. Chem. Chem. Phys.,* 2013, **15**, 11221.

8 S. Yi, S. Tian, D. Zeng, K. Xu, X. Peng, H. Wang, S. Zhang and C. Xie, *Sensor. Actuat. B,* 2014, **204**, 351.

9 I. Rawal, *RSC Adv*. 2014, DOI: 10.1039/C4RA12747A.

10 (a) P. J. Shaver, *Appl. Phys. Lett.,* 1967, **11**, 255. (b) K. Suematsu, Y. Shin, Z. Hua, K. Yoshida, M. Yuasa, T. Kida and K. Shimanoe, *Sensor. Actuat. B,* 2014, **6**, 5319.

11 Y. D. Wang, X. H. Wu, Q. Su, Y. F. Li and Z. L. Zhou, *Solid. State. Electron.,* 2001, **45**, 347.

12 (a) L. Wang, H. Dou, Z. Lou and T. Zhang, *Sensor. Actuat. B,* 2013, **5**, 2686. (b) B. Jang, O. Landu, S. J. Choi, A. Rothschild and I. D. Kim, *Sensor. Actuat. B,* 2013, **188**, 156.

13 X. Wang, H. Qin, Y. Chen and J. Hu, *J. Phys. Chem. C,* 2014, **118**, 28548.

14 Q. Deng, X. Duan, D. H. L. Ng, H. Tang, Y. Yang, M. G. Kong, Z. Wu, W. Cai and G. Wang, *ACS Appl. Mater. Interfaces* 2012, **4**, 6030.

15 (a) Y. Liu, Y. Jiao, Z. Zhang, F. Qu, A. Umar and X. Wu, *ACS Appl. Mater. Interfaces* 2014, **6**, 2174. (b) S. Wang, J. Yang, H. Zhang, Y. Wang, X. Gao, L. Wang and Z. Zhu, *Sensor. Actuat. B,* 2015, **207**, 83. (c) P. Gurunathan, E. Masthaaiah and K. Ramesha, *ACS Appl. Mater. Interfaces,* 2014, **6**, 16556.

16 Y. D. Wang, I. Dgerdj, M. Antonietti and B. Smarsly, *Small,* 2008, **4**, 1656.

17 L. B. McCusker, R. B. Von Dreele, D. E. Cox, D. Louër and P. Sacrdi, *J. Appl. Cryst.,* 1999, **32**, 36.

18 (a) A. Kawska, P. Duchstein, O. Hochrein and D. Atomistic, *ACS Appl. Mater. Interfaces,* 2008, **8**, 2336. (b) S. Xu and Z. L. Wang, *Nano Res*., 2011, **4**, 1013.

19 X. Liu, X. Xing, Y.X. Li, N. Chen and I. Djerdj, Y. Wang, *New J. Chem.,* 2015, 39, 2881.

20 Y. Zheng, L. Zheng, Y. Zhan, X. Lin, Q. Zheng, K. Wei, Inorg. Chem., 2007, 46, 6980.

21 C. Dong, X. Liu, X. Xiao, G. Chen and Y. Wang, I. Djerdj, *J. Mater. Chem. A,* 2014, **2**, 20089.

22 G. Wang, Q. Mu, T. Chen and Y. Wang, *J. Alloy. Compd.,* 2010, **493**, 202.

23 D. Peeters, D. Barreca, G. Carraro, E. Comini, A. Gasparotto, C. Maccato and C. Sada, *J. Phys. Chem. C,* 2014, **118**, 11813.

24 Q. Qi, T. Zhang, L. Liu, X. Zhang and G. Lu, *Sensor. Actuat. B,* 2009, **141**, 174.

25 J. Zhang, S. Wang, M. Xu, Y. Wang, H. Xia, S. Zhang, X. Guo and S. Wu, *J. Phys. Chem. C,* 2009, **113**, 1662.

26 N. V. Hieu, T. B. Thuy and N. D. Chien, *Sensor. Actuat. B,* 2008, **129**, 888.

27 A. V. Anisimov, N. K. Maksimova, E. V. Chernikov, E. Y. Sevastyanov and N. V. Sergeychenko, *IEEE Siberian Conference on Control and Communications,* **2009**.

28 L. Jia, W. Cai and H. Wang, *Appl. Phys. Lett.,* 2010, **96**, 103115.

29 (a) M. Cao, Y. Wang, T. Chen, M. Antonietti and M. Niederberger, *Chem. Mater.* 2008, **20**, 5781. (b) T. Chen, Q. J. Liu, Z. L. Zhou and Y. D. Wang, *Nanotechnology*, 2008, **19**, 095506. (c) T. Wolkenstein, Electronic Processes on Semiconductor Surface during Chemisorption (New York: Consultants Bureau), 1991, 35-182.